JGR Atmospheres

RESEARCH ARTICLE
10.1029/2020JD034130

Potential Impacts of Supersonic Aircraft Emissions on Ozone and Resulting Forcing on Climate: An Update on Historical Analysis

Jun Zhang[1], Donald Wuebbles[1], Douglas Kinnison[2], and Steven L. Baughcum[3]

[1]Department of Atmospheric Sciences, University of Illinois, Urbana, IL, USA, [2]National Center for Atmospheric Research, Boulder, CO, USA, [3]Boeing Company, Seattle, WA, USA

Key Points:

- Nitrogen oxides (NO_x) and water vapor (H_2O) emissions from fleets of supersonic transport (SST) aircraft can potentially affect stratospheric ozone and climate
- New climate-chemistry model analyses of a fleet of SSTs on ozone are similar to results from earlier (1999) aviation assessments, although with a greater sensitivity to NO_x emissions
- Ozone and climate effects from an SST fleet depends on the amount of NO_x and H_2O emissions and resulting chemical interactions through ozone production and depletion catalytic cycles

Supporting Information:

- Supporting Information S1

Correspondence to:
J. Zhang,
jzhan166@illinois.edu

Citation:
Zhang, J., Wuebbles, D., Kinnison, D., & Baughcum, S. L. (2021). Potential impacts of supersonic aircraft emissions on ozone and resulting forcing on climate: An update on historical analysis. *Journal of Geophysical Research: Atmospheres*, *126*, e2020JD034130. https://doi.org/10.1029/2020JD034130

Received 22 OCT 2020
Accepted 15 FEB 2021

Abstract Commercial aircraft flying at supersonic speeds in the lower stratosphere are being discussed once again after a hiatus of almost 20 years. Potential environmental effects from fleets of such aircraft need to be understood for their possible impacts on stratospheric ozone; levels of stratospheric ozone determine the amount of biologically harmful ultraviolet radiation from the Sun reaching the Earth's surface. Changes in the distribution and concentrations of ozone also have implications on climate. This study evaluates the potential impact on stratospheric ozone and on climate forcing from different levels of nitrogen oxides (NO_x) and water vapor (H_2O) emissions from supersonic transport. Toward establishing a baseline relative to prior studies, we also compare these new analyses with results from the 1999 aviation assessments, using the same aviation emissions. Despite the understanding of atmospheric processes used in studying chemistry-climate interactions have been greatly enhanced over the last 20 years, this study finds that, for the baseline scenario, the resulting effects on stratospheric ozone are similar to those from many of the models in the prior assessment, although with a stronger ozone sensitivity to NO_x emissions. We show that the resulting ozone effects largely depend on the NO_x and H_2O emission levels and the net changes in stratospheric ozone are determined by the chemical interactions between different ozone production and depletion cycles. We also calculate the radiative forcing impact for the resulting changes in the distributions of ozone and H_2O, and confirm that stratospheric H_2O emissions are an important factor in potential climate impacts from supersonic aircraft emissions.

Plain Language Summary Emissions from potential fleets of supersonic transport (SST) aircraft have raised concerns about potential effects on stratospheric ozone and climate. This study revisits the ozone and climate impacts from a potential fleet of SST aircraft that were examined in scientific assessments over 20 years ago. This study uses an advanced global atmospheric model to provide a modern baseline relative to the prior analyses. The results show that the derived impact on the distribution of atmospheric ozone are similar to the models used in the earlier analyses. The results also indicate that the effects on ozone and radiative forcing show a strong sensitivity to the particular levels of NO_x and H_2O emissions, and a stronger ozone sensitivity to NO_x emission is found in new analyses compared to prior studies.

1. Introduction

The overall demands by the public for air travel, the aspiration for more intercontinental travel, and the desire for shorter flight times have all increased in the past few decades. As a result, various companies and organizations around the world have been reconsidering development of supersonic aircraft for the business jet and commercial airline markets (e.g., NASA, Aerion, Spike Aerospace, and Boom Technology). Commercial fleets of supersonic transport (SST) aircraft were first considered in the 1970s (Climate Impact Assessment Program, 1975) and then again in the 1990s (Kawa et al., 1999). The cruise altitudes flown by supersonic aircraft depends on the design and speed of the aircraft with faster aircraft flying at higher altitudes. Supersonic aircraft would fly at higher altitudes than the current fleet of subsonic aircraft, with their emissions primarily being in the stratosphere.

With a potential range of cruise altitudes from 13 to 23 km, the majority of emissions from supersonic aircraft would occur in the stratosphere and would have longer atmospheric lifetimes than the emissions occurring from subsonic aircraft that primarily fly in the troposphere. Supersonic aircraft emissions can be

especially of concern because of potential effects on stratospheric ozone and also on climate. The exhaust emissions from SST aircraft, which would be expected to use jet fuel, much like their subsonic counterparts, include carbon dioxide (CO_2), nitrogen oxides (NO_x), water vapor (H_2O), sulfate, hydrocarbons and soot. Fuel sulfur content would influence the sulfate particle production, although this production from SST is highly uncertain (Fahey et al., 1995). Other emissions like hydrocarbon and soot are small; their emissions are unlikely to have important stratospheric effects on ozone. NO_x and H_2O (after reaction to form hydrogen oxides; HO_x) are known to be important gases in the chemical production and destruction of stratospheric ozone. Both NO_x and HO_x can be directly involved in catalytic chemical reactions that destroy molecules of stratospheric ozone, both from natural and human-related sources like supersonic aircraft (e.g., Crutzen, 1972; Dessens et al., 2007; Johnston, 1971, 1989; Kawa et al., 1999; Kinnison & Wuebbles, 1994; Kinnison, Brasseur, Baughcum, et al., 2020; Penner et al, 1999). Emissions of NO_x and HO_x can interfere with each other's ozone-loss mechanisms and they can also interfere with other ozone-loss mechanisms (e.g., ClO_x). As a result, the net effect of this interference can be a local increase in stratospheric ozone. The net effect depends on the amount of each emission and the altitude of the emissions. The net effect on the global ozone distribution depends on the complex interactions between nitrogen oxides, hydrogen oxides, and the amounts of chlorine, bromine, and other gases in the stratosphere (World Meteorological Organization, 2018). Potential climate concerns from SST emissions arise both from the direct effects of CO_2 and H_2O emissions; and from the indirect effects on the distribution of atmospheric ozone.

The most recent prior studies on the environmental effects from potential supersonic aircraft emissions date back to more than 10 years ago. Of particular relevance is a series of research studies (e.g., Dameris et al., 1998; Grewe, Plohr, et al., 2010; Grewe, Stenke, et al., 2007; Grooß et al., 1998; Johnston et al., 1989; Kinnison, Connell, et al., 2001). There are also assessment reports resulting from NASA's Atmospheric Effects of Aviation Project (AEAP; Kawa et al., 1999), and a special international Intergovernmental Panel on Climate Change (IPCC) assessment on aviation impacts on climate (Penner et al., 1999). Later studies from SCENIC (Scenario of aircraft emissions and impact studies on chemistry and climate) and HISAC (Environmentally friendly High Speed Aircraft) projects also explored the environmental effects from supersonic air traffic. SCENIC and HISAC assumed specific aircraft concepts to develop different emission scenarios relative to those used in the NASA and IPCC assessments (Grewe, Plohr, et al., 2010; Grewe, Stenke, et al., 2007). In this study, the emission scenarios from the NASA and IPCC assessments are used. In these two earlier assessments, 10 atmospheric models from that era were used and the assessments made a comprehensive comparison. This study uses these old emission scenarios to examine the potential impacts on ozone and climate forcing with a current state-of-the-art chemistry-climate model.

The NASA and IPCC assessments assumed a specific design for a SST known as the High Speed Civil Transport aircraft (HSCT); this was a large (300 passenger), long range (5,000 nautical mile), Mach 2.4 SST aircraft. The HSCT was aimed at being much larger, faster, and longer range than the earlier Concorde aircraft or, for that matter, most supersonic aircraft now being discussed. For the 1999 assessments, HSCTs were projected to have fleets of 500 and 1,000 aircraft by the year 2015. At the time of the assessment, three of the models were early generation three-dimensional (3-D) models that had limited representations of stratospheric chemistry and physics, and the other seven participating models in the assessments were zonally averaged two-dimensional (2-D) models. Also, the 2-D models in 1999 were the primary tools for studying stratospheric ozone, in large part because of computational limitations slowing the development of 3-D models. Since then, computers have become much faster and 3-D models have matured. At this time, because of their limitations, 2-D models are seldom used, while 3-D models are now the workhorses for studies of stratospheric processes.

There has been a substantial increase in the understanding of tropospheric and stratospheric physical and chemical processes over the last 20 years, including better representation of transport processes with higher resolution, especially near the tropopause; improved understanding of the processes affecting water vapor in this region; and improved microphysics parameterizations affecting particle distributions (e.g., as summarized in the array of WMO stratospheric ozone assessments and IPCC assessments, including the most recent, IPCC, 2013; WMO, 2018). As a result, there has been a substantial increase in the ability to accurately evaluate the potential effects of HSCTs on ozone and climate. Given the renewed interest in fleets of supersonic aircraft, we have chosen to revisit the issue of the impact of supersonic aircraft on the ozone

layer, starting with reestablishing the baseline for such studies relative to the assessment studies that were done roughly 20 years ago.

This study is focused on NO_x and H_2O emissions from fleets of supersonic aircraft and their potential impacts on atmospheric ozone and the resulting forcing on climate. In this paper, we directly update the earlier evaluations by using the same emission scenarios that were used in the earlier NASA and IPCC assessments. By establishing a baseline relative to the earlier studies, the aim in this study is to see how the effects of a HSCT fleet is now determined in a current state-of-the art three-dimensional atmospheric chemistry-climate model in comparison to the results from the two 1999 assessments. This study also evaluates the potential response on ozone and climate from different levels of NO_x and H_2O emissions toward examining the effects on the different catalytic cycles by separating the effects of the different catalytic ozone loss cycles. The purpose is to provide a baseline for future considerations of potential fleets of supersonic aircraft.

2. Methodology

2.1. Model Description

2.1.1. WACCM4

The Community Earth System Model/Whole Atmosphere Community Climate Model version 4 (CESM/WACCM4) is a fully coupled interactive chemistry-climate model for the global atmosphere (Marsh et al., 2013). WACCM extents from the Earth's surface to well into the thermosphere, with a top altitude of 6.0×10^{-6} hPa (~140 km), and it fully represents chemical and physical processes in the troposphere, stratosphere, and above. Models dealing with supersonic aviation should include the whole stratosphere in order to represent the age of air masses in the stratosphere correctly. WACCM includes a comprehensive global atmosphere that fully represents tropospheric and stratospheric chemical processes making it a unique tool to evaluate the environmental effects of supersonic aircraft. In this study, all WACCM simulations have a horizontal resolution of 1.9° latitude × 2.5° longitude over 66 vertical levels. The vertical resolution is ~1.2 km in the lower stratosphere below 30 km, ~2 km around the stratopause (~50 km), and ~3 km in the mesosphere and thermosphere. The vertical resolution in the troposphere is ~1 km, except with higher resolution near the ground.

The chemical scheme of WACCM4 is updated relative to the previous chemical transport Model for OZone And Related chemical Tracers 3 (MOZART) (Kinnison, Brasseur, Walters, et al., 2007), with chemical kinetics and photochemical rate constants updated to the JPL-2010 recommendations (Sander et al., 2010), while the much earlier JPL97 chemistry rate recommendations (DeMore et al., 1997) were used in the modeling studies for the NASA AEAP and IPCC assessment calculations. The species included in WACCM include all of the key source gases affecting the ozone chemistry, along with methane and its degradation products. In addition, 20 primary non-methane hydrocarbons and related oxygenated organic compounds are represented along with their surface emissions. The chemical mechanism also includes the gas phase and heterogeneous reactions on liquid binary and ternary sulfate polar stratospheric cloud (PSC) particles, as well as solid nitric acid trihydrate and water ice polar stratospheric particles. These chemical reactions are all necessary to fully represent atmospheric ozone chemistry. A total number of 183 species associated with 472 chemical reactions are included in the model.

The WACCM4 model has been extensively used and evaluated, including its ability to accurately represent stratospheric ozone and polar ozone processes (Garcia, Smith, et al., 2017; Kunz et al., 2011; Marsh et al., 2013; Solomon et al, 2015, 2016; Wegner et al., 2013). Froidevaux et al. (2019) have evaluated the stratospheric ozone, H_2O, HCl, N_2O, and HNO_3 derived from WACCM4 with observations in terms of their trends and abundances as well as longer-term series. The model derived trends and abundances are evaluated using the near-global stratospheric data set of the Aura Microwave Limb Sounder (MLS) in the time period from 2005 to 2014. The data sets from the Global OZone Chemistry And Related trace gas Data records for the Stratosphere (GOZCARDS) are used for the evaluation of longer-term series before the launch of Aura (Froidevaux et al., 2015; Livesey et al., 2015; Wang et al., 2013). Results show that the stratospheric ozone trends from WACCM agree well with the MLS trends, with most of the modeled ozone climatology being within 5%–10% of the data climatology. For H_2O, WACCM and MLS both show similar short-term positive trends and the abundances also agree well—within ~5% and ~10% difference in the stratosphere

and mesosphere respectively. For HCl, N_2O, and HNO_3, the short-term trend profiles from MLS are well captured and matched by WACCM trends for these species in the stratosphere.

The middle atmospheric dynamics (e.g., temperature, zonal winds) have also been evaluated relative to observations from previous studies (Froidevaux et al., 2019; Garcia, Yue, et al., 2019; Marsh et al., 2013). The temperature distribution derived from WACCM has been found to compare well to the temperature obtained from the Sounding of the Atmosphere using the Broadband Emission Radiometry (SABER) instrument on the Thermosphere, Ionosphere, Mesosphere Energetics and Dynamics (TIMED) satellite (Remsberg et al., 2008); WACCM well captures the pattern of the warm and cool peaks in the stratosphere and mesosphere both in summer and winter. Garcia, Smith, et al. (2017) has also examined the annual stratospheric temperature in the Southern Hemisphere polar region (−90° to −69°) derived from WACCM and compared it to Modern-Era Retrospective analysis for Research and Applications (MERRA) data; this analysis indicated that WACCM reproduces the seasonal variations for stratospheric temperature. This is important in calculating the perturbation to PSCs from injected water vapor from supersonic aircraft. The derived zonal mean wind fields from WACCM also indicate good agreement with the Upper Atmosphere Research Satellite (UARS) Reference Atmosphere Project (URAP) climatology (Swinbank & Ortland, 2003) data set for the same time period (Marsh et al., 2013). Marsh et al. (2013) also indicates that WACCM well represents the quasi-biennial oscillation (QBO) in the stratosphere, which is important to ozone representation, and the semi-annual oscillation (SAO) in the mesosphere, which dominates the behavior of mesospheric wind fields.

The treatments of chemistry and physical processes in WACCM are greatly improved relative to the earlier models used in the 1999 assessments (Kawa et al., 1999). WACCM incorporates a more physically realistic representation of the atmospheric dynamics and circulation processes, including much improved representations for microphysics and planetary waves. WACCM can explicitly resolve the transport processes in the upper troposphere and lower stratosphere while the earlier 2-D and 3-D models primarily relied on diffusive vertical mixing parameterizations. In addition, the higher horizontal and vertical resolution in WACCM also results in a more realistic residual circulation. This is important; the time scale of mass flux across the extratropical tropopause into the troposphere is dominantly driven by the wave breaking process in the lower stratosphere (Gettelman et al., 1997; Holton et al., 1995; Shepherd et al., 2011). The rate of this stratosphere to troposphere exchange determines the accumulation of HSCT emissions in the middle and upper stratosphere, and thereby affecting the resulting impacts on stratospheric ozone.

In addition, there is a significant improvement in the model treatment of stratospheric water vapor in WACCM. The earlier models from the two assessments constrained water vapor to climatological measurements at the tropopause, and thus defined the H_2O sink and removal processes only by this boundary condition. WACCM can calculate H_2O explicitly and thus responds to H_2O perturbations from supersonic aircraft in a more physically complete process.

2.1.2. The Parallel Offline Radiative Transfer Model (PORT)

We also use the PORT model (Conley et al., 2013), a configuration of the Community Atmosphere Model (CAM) in the CESM which runs the radiative transfer code offline. Using the same framework as CAM, PORT is able to reproduce the same heating rates and longwave and shortwave fluxes as those in CAM. Furthermore, the model uses seasonally evolving fixed-dynamical heating (Fels et al., 1980) to determine temperature adjustments and stratospheric-adjusted radiative forcing at the tropopause (IPCC, 2013) associated with perturbations in chemical constituents. PORT uses instantaneous samples of the model state to compute radiative fluxes and heating rates without feedbacks on surface, subsurface, and atmospheric states. The radiation parameterization computes absorption, scattering, emission effects of shortwave solar radiation and longwave infrared radiation by the atmosphere and surface. PORT has been widely used and tested with CESM-generated data sets (e.g., Conley et al., 2013; Ivy et al., 2017; Lamarque et al., 2011; Polvani et al., 2020; Wang & Huang, 2020), and have been implemented to calculate both instantaneous radiative forcing and radiative forcing including stratospheric temperature adjustment. PORT is used in this study to examine the radiative forcing on climate of the H_2O and ozone perturbations from the assumed HSCT emissions. This radiative forcing includes the stratospheric temperature adjustment, which allows the stratospheric temperature to adjust to radiative equilibrium in the system above the tropopause under the assumption of fixed dynamical heating.

Table 1
Emission Scenarios for HSCT Study in a 2015 Background Atmosphere

Case	Fleet size	Fuel burn (Tg/yr)	Cruise altitude (km)	NO_x emission index (g/kg)	H_2O emission index (g/kg)
A	500	47.25	17–20	5	1,237
B	500	47.25	17–20	10	1,237
C	500	47.25	17–20	15	1,237
D	500	47.25	17–20	15	0
E	500	47.25	17–20	0	1,237
F	1,000	83.76	17–20	5	1,237

2.2. Model Simulations and Emission Scenarios

The WACCM simulations in this study are forced by specified sea surface temperature and sea ice boundary conditions, and by observations of the evolution of long-lived chemical species at the Earth's surface (following the approach of Morgenstern et al., 2017). The simulation was started in model year 2005 and run for 12 years until reaching a steady-state. After reaching steady-state, the annual ozone concentration fluctuates with the variation of the QBO phase and due to seasonal variations, but does not otherwise change year to year. The model is run in specified dynamics mode with the meteorology fields externally nudged to the free running simulation. Source gas boundary conditions used for the 2015 background atmospheres are based on the Coupled Model Intercomparison Project Phase 5 with improvements in the latitudinal and seasonal gradients (Meinshausen et al., 2011). For each set of simulations, the model was driven with the same meteorology fields, kinetic reactions and rates, heating rates, and climatology files yet differing aircraft emission input files according to the scenarios studied. Reference runs are first performed for a 2015 background atmosphere in which the supersonic aircraft emissions are excluded. Then the experiment runs are conducted by adding supersonic perturbations on top of the background atmosphere. For the HSCT scenarios evaluated in this study, all of the results are evaluated once the model has reached steady state relative to the prescribed background atmosphere. All the simulations include the effects of the QBO, which is nudged to the observed tropical winds (Matthes et al., 2010) and the meteorological fields are nudged up through 120 km altitude. The results from the last three years are used in the analysis due to the slightly different effects on ozone for the different phases of the QBO. The difference between the perturbed and reference background simulations are the changes induced from the supersonic aircraft emissions.

The assumed HSCT aircraft was a conceptual 300-passenger supersonic aircraft with a maximum range of 5,000 nautical miles. The aircraft was projected to cruise supersonically at Mach 2.4 between 17 and 20 km altitudes. The aircraft were assumed to fly supersonically only over water due to concerns about noise from sonic booms over-populated regions; as a result, operations for long-range international transport routes are projected to primarily cross the Atlantic and Pacific Oceans based on market analyses. A selection of emission scenarios with different assumed fleet sizes and NO_x emission indexes from Kawa et al. (1999) are chosen to evaluate the sensitivity of the response to market size and combustor technology. Case A–E in Table 1 lists all the emission scenarios used in this study. For these simulations, we do not consider sulfate emissions by the aircraft which is equivalent to assuming zero sulfur jet fuel. Those emission inventories were originated and developed by Boeing as a progression from previous studies (Baughcum & Henderson, 1995, 1998; Baughcum et al., 1994). For fleets of 500 and 1,000 HSCTs, the total global fuel use and emissions from these scenarios are summarized in Table 1.

Emission indices of NO_x and H_2O stand for the amount of NO_x and H_2O emitted in g/kg fuel burn. NO_x emissions are given on an NO_2 equivalent mass basis. NO_x is formed during the combustion process through high-temperature reactions between molecular nitrogen and oxygen. An emission index (EI) of 0, 5, 10, 15 g of NO_x/fuel burn are evaluated in this study (Case A–C and E). The H_2O emission level is proportional to the fuel burn and is assumed to be EI (H_2O) = 1,237 g H_2O/kg fuel burn. Experiments also have been conducted to look at H_2O or NO_x emission only scenarios. Cases D and E explore their relative contribution to ozone changes and the chemical interactions between H_2O and NO_x. Case F explores the resulting ozone impact when doubling the number of aircraft in operation. Case A is the baseline emission scenario in this study. These scenarios were calculated on a 1° latitude by 1° longitude by 1 km pressure-altitude grid and then interpolated onto the computational grids of the WACCM model.

The geographical distribution of fuel use at cruise altitude is shown in Figure 1 for a fleet size of 500 HSCTs. Fuel burn is concentrated in a midlatitude flight corridor resulting from the market projection of where the major demand for such an aircraft would be. The majority (~84%) of fuel burn occurs in the Northern Hemisphere (NH) and around 62% is between 30°N to 60°N.

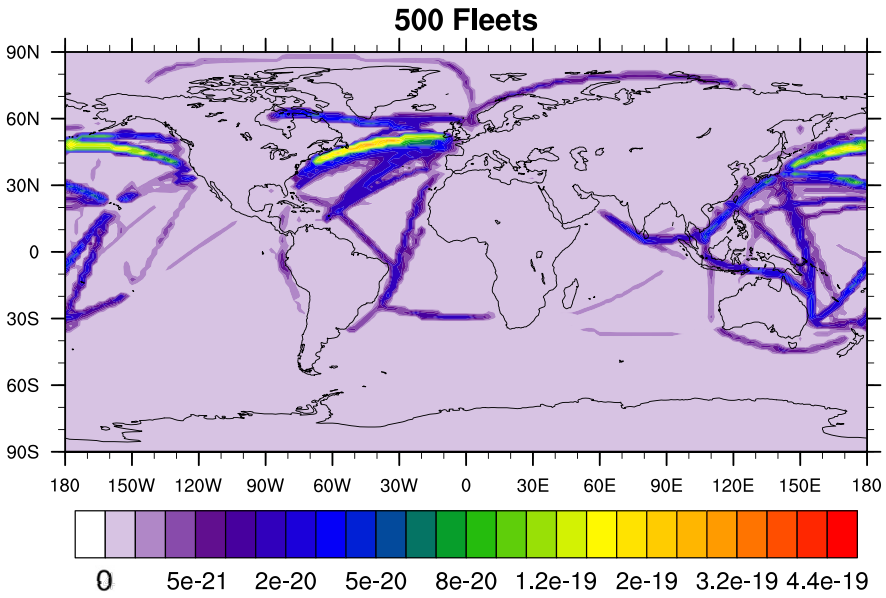

Figure 1. Projected distribution of fuel usage (kg/cm^2/s) vertically integrated at cruise altitudes for the assumed fleet of 500 supersonic aircraft.

3. Source Gases and the Resulting Background Atmosphere

Source gas boundary conditions at the Earth's surface adopted in this study are found in Table S1, with available values for corresponding species from the 1999 NASA assessment also listed for comparison. The distribution of these source gases in the background atmosphere is determined by a combination of chemistry and transport processes. The ozone impact depends strongly on the background atmosphere at the locations where the aircraft are flying. The reference background atmosphere assumed in this study includes a subsonic fleet and a sulfate surface area density that is representative of a volcanically clean atmosphere.

Examining ozone sensitivity to a NO_x disturbance requires the good representation of the total odd nitrogen (NO_y) budget in the lower stratosphere, since it provides basis for the amount of NO_y converted into more reactive nitrogen NO_x (where NO_y is defined as the sum of N + NO + NO_2 + NO_3 + HO_2NO_2 + HNO_3 + $2N_2O_5$ + ClO-NO_2 + minor contributions from other nitrogen species, whereas NO_x is comprised of NO + NO_2). Park et al. (2017) evaluated the NO_x and NO_y derived from WACCM relative to satellite observations from the Optical Spectrograph and Infrared Imager System (OSIRIS) instrument, and found a close agreement between the satellite observations and model-derived concentrations. They also provided quantitative comparisons of nitrogen partitioning and ozone sensitivity to NO_x and found an overall good agreement except that the model show larger (up to 20%) variations in N_2O, NO_x and ozone at around 35 km altitude compared to the observations. WACCM derived background N_2O and NO_y profiles for 1992 conditions are also compared against previous climatological aircraft observations from Strahan (1999) in Figure 2 to compare with previous model performance. The vertical profiles of N_2O and NO_y from WACCM at midlatitudes shows good agreement with the climatology in summer, much better than the comparison of these observations to the models used in the 1999 NASA and IPCC assessments (see Figure S1; a list of the models used in the 1999 NASA and IPCC assessments can be found in Table S2). These analyses indicate that WACCM has a better representation of atmospheric circulation, mixing, troposphere-stratosphere exchange and chemistry, as these factors together determine the vertical profile of N_2O and NO_y. Figure 3a shows the WACCM derived annual and global average in background ratio of NO_x to NO_y for the assumed 2015 conditions. The ratio of NO_x to NO_y is around 15% near the HSCT cruise altitude and the ratio increases with rising altitude. Additional NO_x from HSCT emission can alter the chemical cycling within the NO_y family through non-linear heterogeneous chemistry. This can further impact ozone chemistry by interfering with other ozone loss cycles in the lower stratosphere.

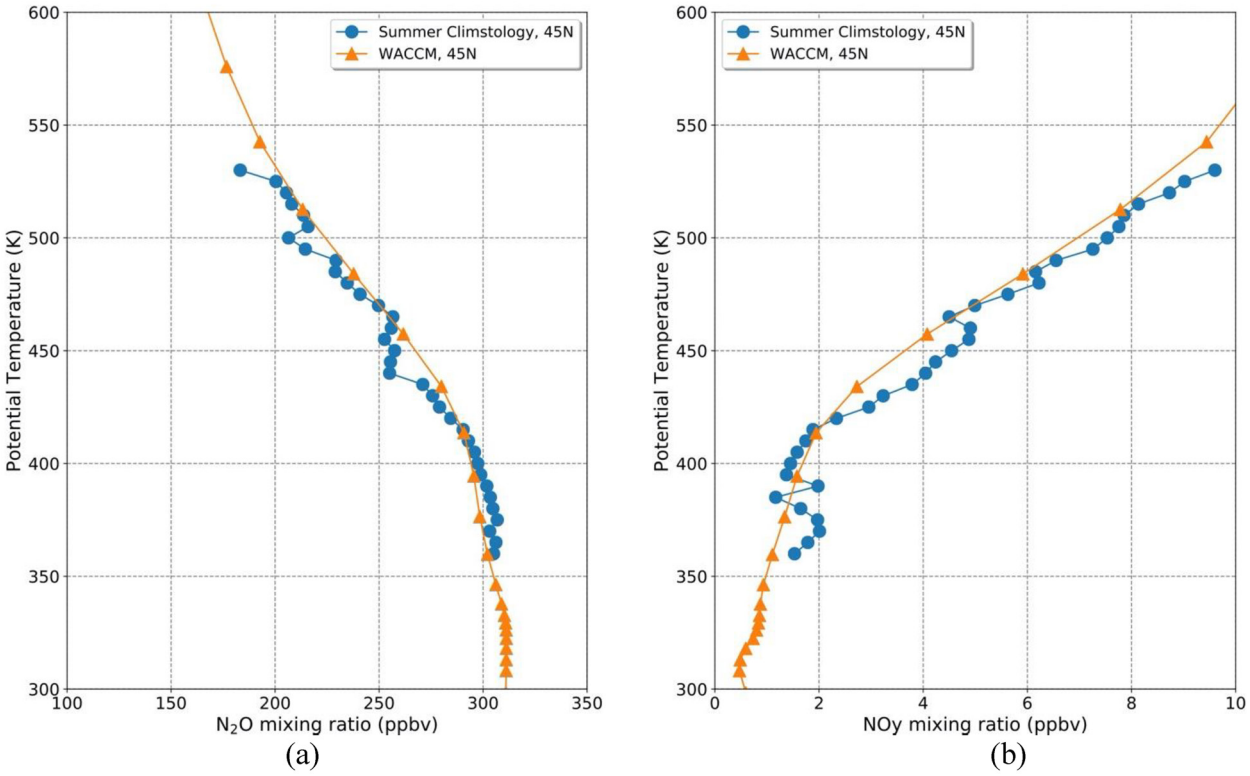

Figure 2. Comparison of WACCM calculated (a) N_2O and (b) NO_y vertical profiles with potential temperature for 1992 model conditions with climatological N_2O and NO_y profiles derived from all ER-2 flights from Strahan (1999) at 45°N, summer season.

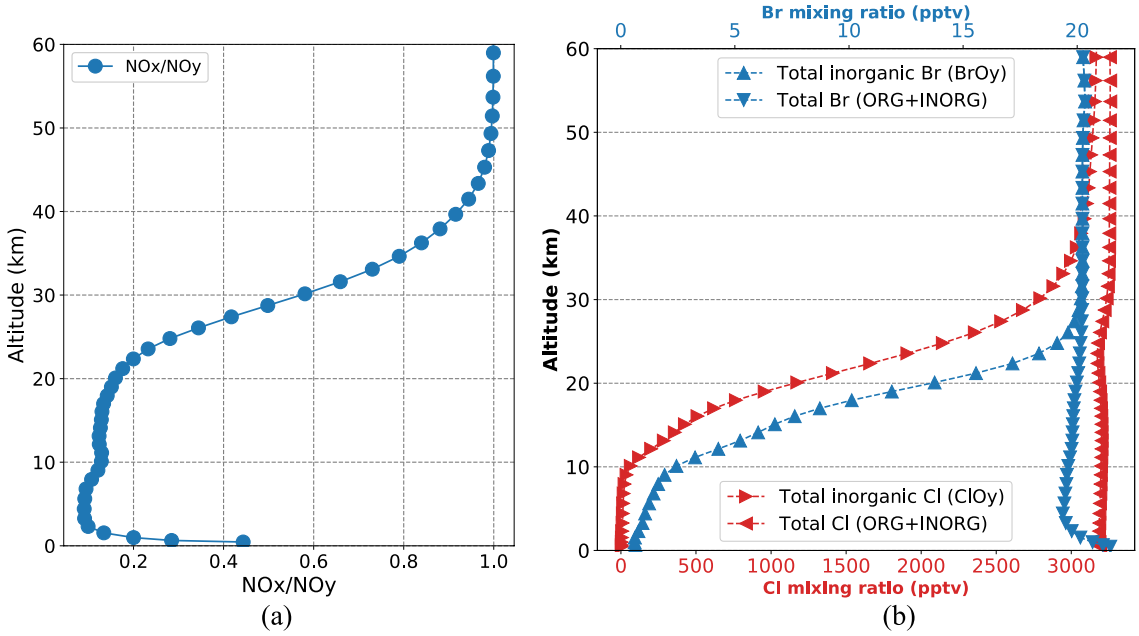

Figure 3. Left panel (a): WACCM derived annual and global average in ratio of NO_x to NO_y for year 2015; right panel (b): total inorganic chlorine (ClO_y) and bromine (BrO_y) and the corresponding total Cl and Br (organic + inorganic) as the function of altitudes in year 2015. Cl mixing ratio is shown in red with the lower labels while Br mixing ratio is in blue with the upper labels.

Background atmospheric levels of chlorine and bromine can also affect the ozone perturbation from the HSCT fleet. Figure 3b shows the model derived global averaged chlorine and bromine mixing ratio changes with altitude for the assumed 2015 conditions. Both the total species of Cl and Br (organic + inorganic), as well as the total inorganic species of ClO_y and BrO_y are shown in Figure 3b. WACCM derives a level of 3.2 ppbv total inorganic chlorine ClO_y (i.e., Cl + ClO + $2Cl_2$ + $2Cl_2O_2$ + OClO + HOCl + $ClONO_2$ + HCl + BrCl) and 20 pptv total inorganic bromine BrO_y (i.e., Br + BrO + HOBr + $BrONO_2$ + HBr + BrCl), respectively at the top of the stratosphere, which are in good agreement with balloon-borne and airborne observations from multiple stations illustrated in the latest ozone assessment (e.g., Kloss et al., 2014; Prinn et al., 2018; Werner et al., 2017; WMO, 2018). The values from WACCM are higher than those adopted in the models from the earlier NASA assessment, which assumed a stratospheric chlorine level of 3 ppbv and a stratospheric bromine level of 12.5 pptv. The BrO_y level in WACCM has a contribution from the very short-lived bromine species (bromoform and dibromomethane), which were not included in the earlier assessments, adding an additional 5 pptv to the stratospheric burden. These factors discussed above can potentially affect the resulting ozone perturbations given the non-linear behavior of heterogeneous processes and the formation of polar stratospheric clouds.

4. Results and Discussion

4.1. NO_y and H_2O Abundances Induced From Assumed HSCT Emissions

The model derived ozone impact from HSCT emissions is directly related to the NO_y and H_2O perturbation accumulated in the model. The calculated changes in the distributions of NO_y and stratospheric H_2O in WACCM due to the assumed HSCTs emissions are shown in Figure 4. Only stratospheric H_2O change is shown here due to the large variability in the troposphere. Panel a and b in Figure 4 show the NO_y and stratospheric H_2O change in June 2015 for Case A (a fleet of 500 HSCTs, $EINO_x = 5$). A distinct increase in the NO_y and H_2O concentrations is found in the lower stratosphere, around 16–20 km (near where emissions occur), for the NH middle to high latitudes. The maximum increases in concentrations of NO_y and H_2O is around 1.1 ppbv and 0.7 ppmv, respectively for Case A. Comparing these results with Figures 4–7 and 4–8 from the 1999 NASA assessment (Figure S2 and S3), the pattern in NO_y and H_2O perturbations derived by WACCM is quite similar to many of the earlier models, with the closest quantitative findings being found in the GSFC-2D and LLNL-2D models for Case A.

Comparing across different emission scenarios in Figure 4c, the majority of the NO_y increase in all cases takes place where most of the emission occurs in the NH lower stratosphere. The maximum perturbation in WACCM increases from 1.1 to 2.2 and 3.2 ppbv locally as increasing the NO_x emission index from 5 to 10 and 15 g/kg fuel burn (Figure S4). Larger amount of NO_y is being transported southward to the tropics and lifted upward to middle stratosphere as the HSCT fleet NO_x injection is increased. There is no NO_y perturbation for the H_2O only case. The NO_y perturbation also increases when doubling the fleet size from 500 to 1,000 HSCTs, while the increase is not as large as the Case B ($EINO_x = 10$); this is due to the fuel use increasing by a factor of 1.8 and therefore is not doubled. The stratospheric H_2O concentration increases shown in Figure 4d indicates similar patterns as NO_y. The largest perturbation in H_2O occurs in the NH lower stratosphere, while noticeable amounts of H_2O reach the upper stratosphere and the SH. This increase in concentration is consistent across different emission scenarios assuming a fleet of 500 HSCTs since these have essentially the same H_2O emissions.

4.2. HSCT Fleet Emission Effects on Ozone

Figure 5 shows the derived changes in the ozone distribution in response to the NO_x and H_2O emissions from the assumed HSCT fleets. For Case A in Figure 5a, between 7 and 17 km at high latitudes and 15–25 km in the tropics, the ozone concentration increases due to the NO_x and H_2O emissions. Above 17 km at high latitudes and 25 km in the tropics, the ozone concentration begins to decrease. The maximum and minimum ozone change both occur at high latitudes but at different altitudes, with the local peak ozone production and reduction being +1.4% and −1.2% at around 11 and 22 km, respectively. The models used in the 1999 NASA and IPCC assessments (Kawa et al., 1999; Penner et al., 1999) have a similar ozone increase and decrease pattern with altitude relative to WACCM (see Figure S5), but the range and magnitude of the

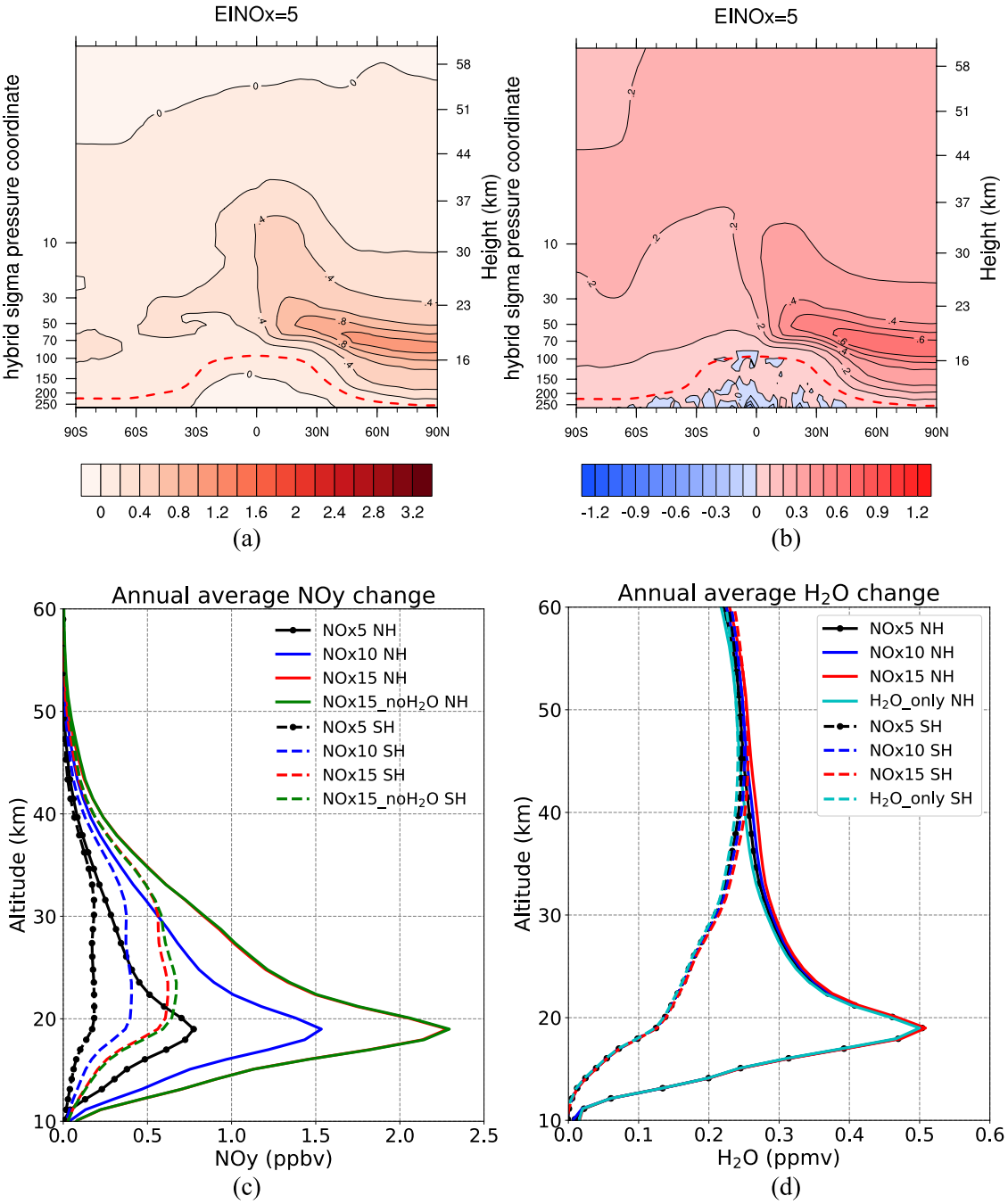

Figure 4. Top panels: Calculated HSCT induced change in (a) NO_y (ppbv) and (b) stratospheric H_2O (ppmv) from WACCM for baseline emission scenario (Case A) during June. The red dashed line indicates the location of the lapse rate tropopause. Bottom panels: Vertical profile of annual average change in (c) NO_y and (d) H_2O for Case A and comparison to other emission scenarios. The baseline emission scenario is shown in black lines with circles. Solid lines are the Northern Hemispheric (NH) average profiles, while dashed lines are the Southern Hemispheric (SH) averages. The red line (NO_x15 SH) is overlapped with the green line (NOH_2O SH) in Figure 4c.

local ozone change varies between the different models used in the earlier assessments. This is likely largely related to differences in the representation of physical processes and odd-oxygen loss partitioning between the NO_x, HO_x, and ClO_x, and BrO_x chemical families between the models.

The vertical profile of Northern Hemispheric annual average ozone change is shown in Figure 5b. Increasing levels of ozone near the tropopause can be found in all of the WACCM scenario cases, except for the H_2O

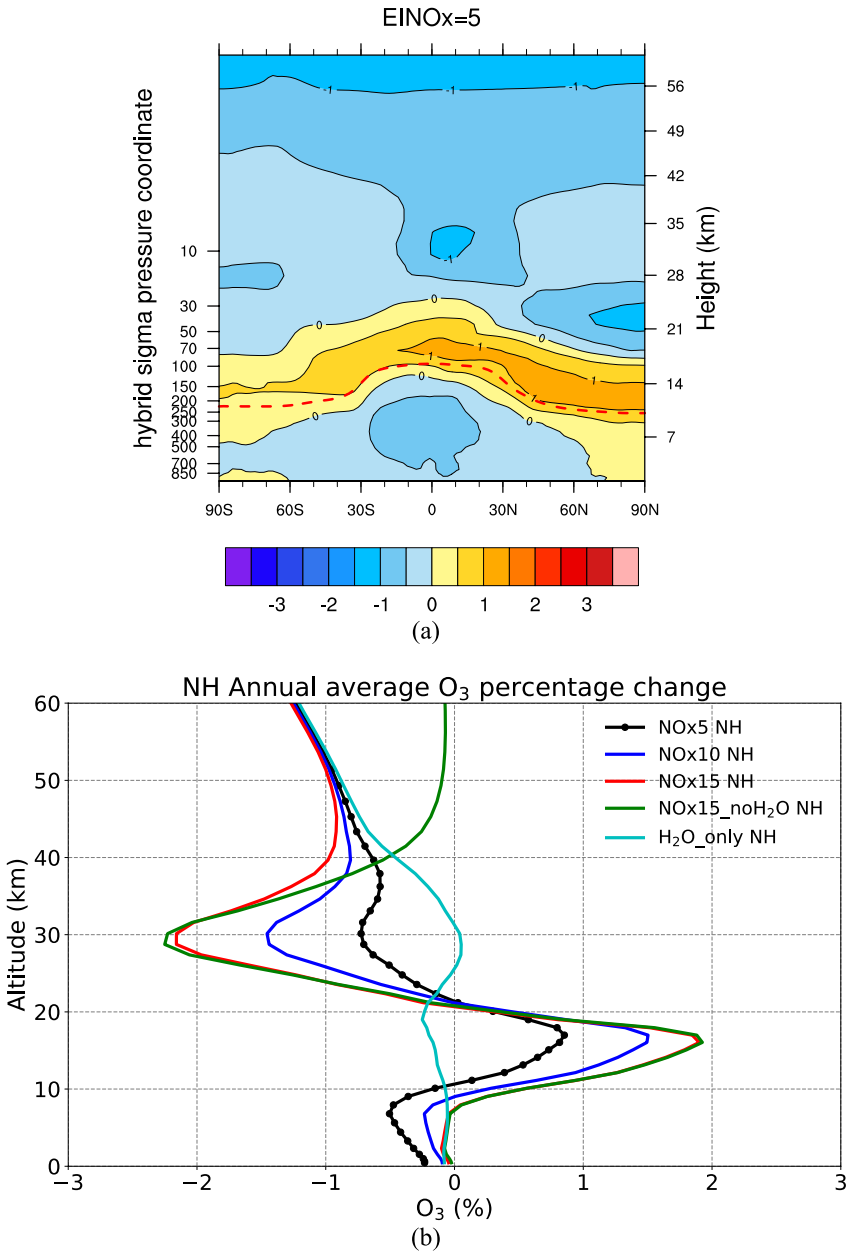

Figure 5. Panel (a): Calculated HSCT induced percentage change in the ozone distribution (%) for baseline emission scenario (Case A) during June. Panel (b): Vertical profile of Northern Hemispheric annual average change in ozone for Case A and comparison to other emission scenarios.

emissions only case. The increases in ozone are extended to the ground at midlatitudes to high-latitudes in both hemispheres (Figure S6). The cross over point in the changes in ozone is around 21 km for the baseline scenario averaged over the NH, with the positive perturbation below and negative perturbation above. The ozone increase near the tropopause is mainly attributed to the HSCT NO_x emissions enhancing the NO_x-ozone production through smog chemistry. In addition, a decrease in the ozone loss rates in this region due to the interference of the emitted NO_x with the HO_x ozone loss cycle also contributes to this ozone increase (Figure S7).

Ozone depletion can be found both below and above the zone of ozone increase at higher latitudes. The ozone depletion above this increase zone is primarily due to the catalytic cycles connected with NO_x and HO_x, and the magnitude of local destruction increases with increasing NO_x emission level. The relatively

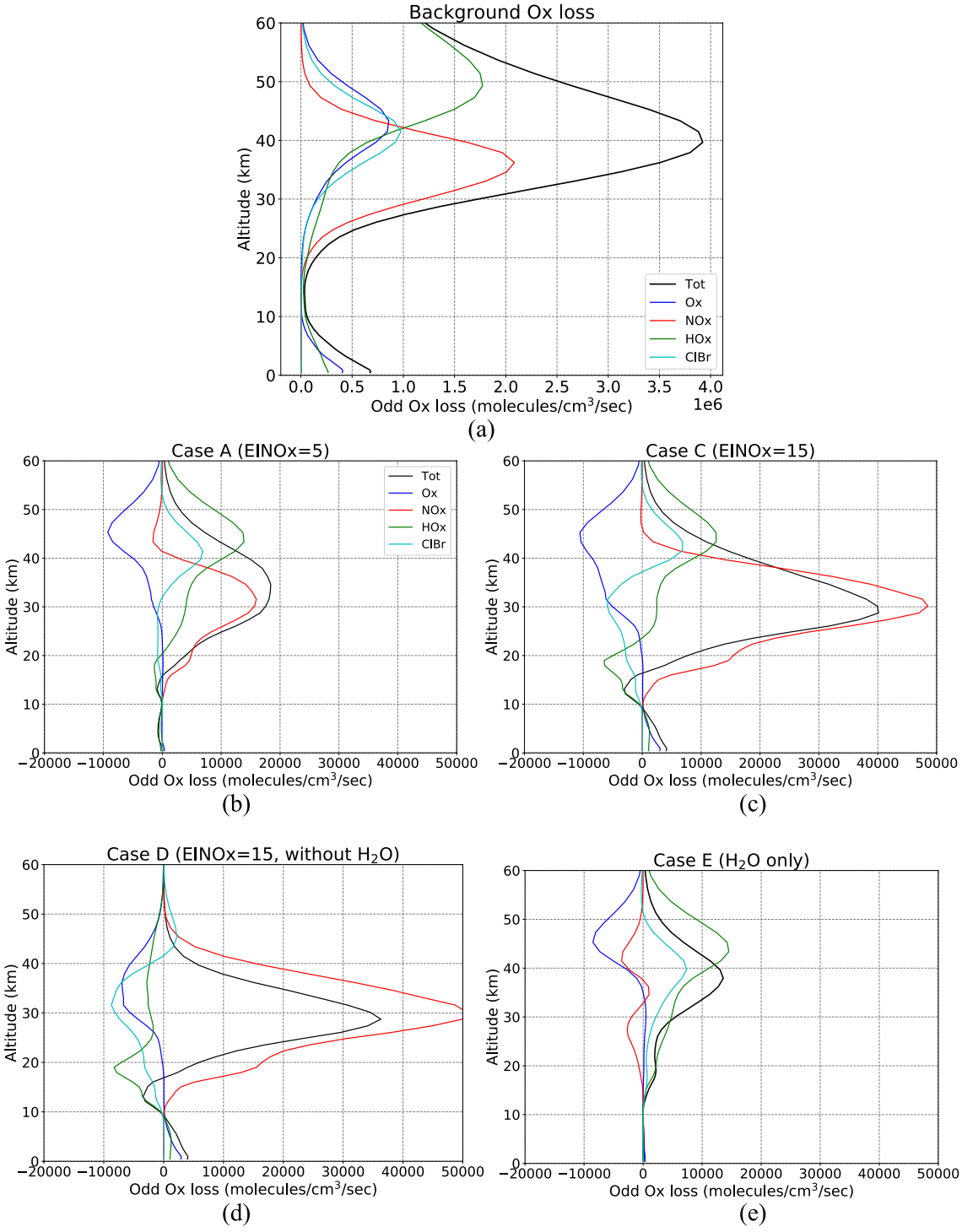

Figure 6. Northern Hemisphere annually averaged profile of odd oxygen (O_x) chemical loss rates by catalytic cycles involving NO_x, HO_x, and halogens as well as the chemical loss by the Chapman mechanism O_x for background condition without HSCTs emissions (panel a) and changes of emission scenarios A C, D, and E (perturbations – background). Different color lines represent different O_x loss mechanisms. The total O_x loss from all the mechanisms is shown in black lines.

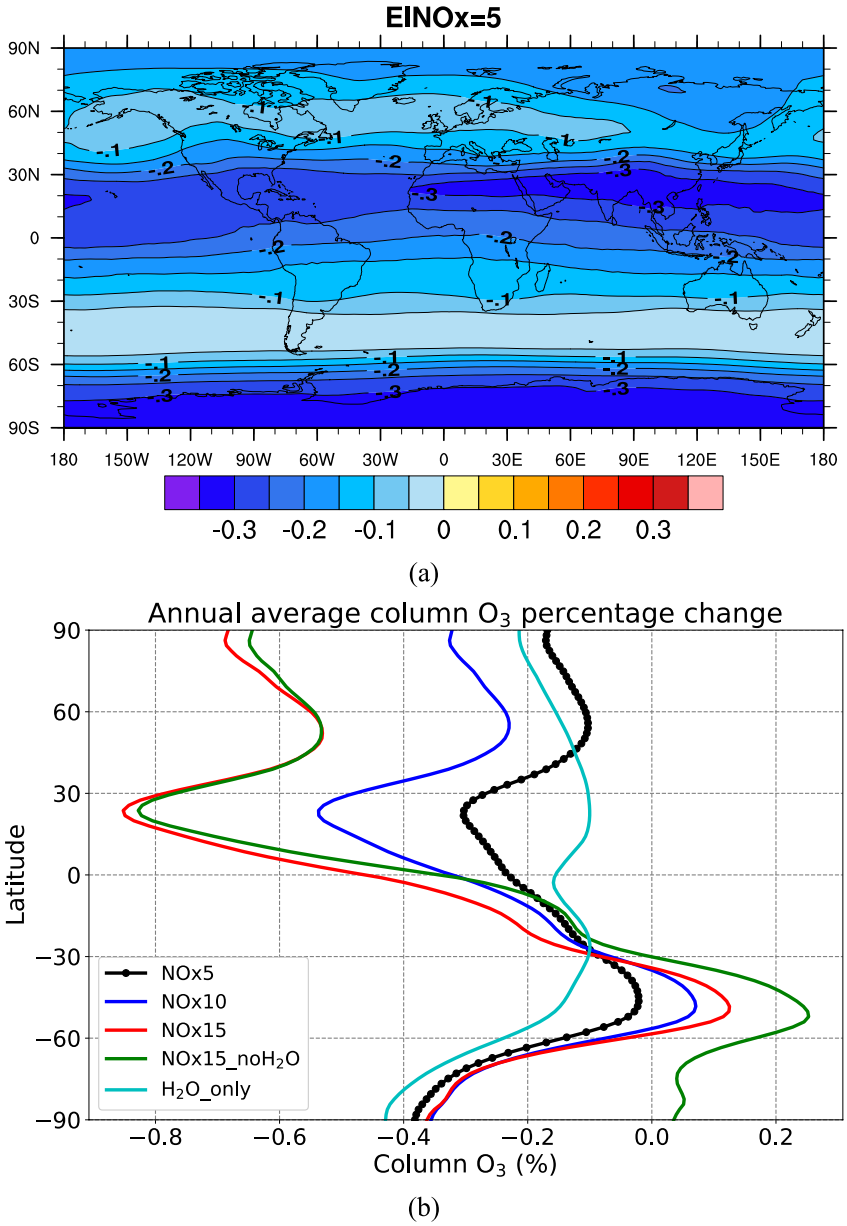

Figure 7. Annually averaged changes in total column ozone (%) for (a) baseline emission scenario (Case A); (b) zonal average change for Case A and comparison to other emission scenarios. The baseline emission scenario is shown in black lines with circles.

small depletion below the ozone increase zone can be found near the tropical region. This primarily results from the self-healing effect, where more radiation is absorbed by the ozone increase above leaving less getting into the troposphere where ozone is produced. The peak percentage in local ozone loss occurs at the northern high latitudes between 21 and 25 km for all cases except the H_2O emission only case. For the H_2O emission only case, the ozone perturbation in the stratosphere is relatively small compared to the other cases that include the HSCT NO_x emissions.

In order to evaluate the relative contribution from NO_x and H_2O emissions to the total ozone loss, odd oxygen ($O_x = O(^3P) + O(^1D) + O_3 + NO_2 + 2NO_3 + HNO_3 + HO_2NO_2 + 2N_2O_5 + ClO + 2Cl_2O_2 + 2OClO + 2ClO\text{-}NO_2 + BrO + 2BrONO_2$) chemical loss by different loss cycles is shown in Figure 6. The cycles used in this study include the loss by NO_x, HO_x, and halogen oxides (ClO_x and BrO_x, which are combined here to show interactions relative to the NO_x and HO_x cycles) catalytic cycles as well as by the Chapman self-destruction

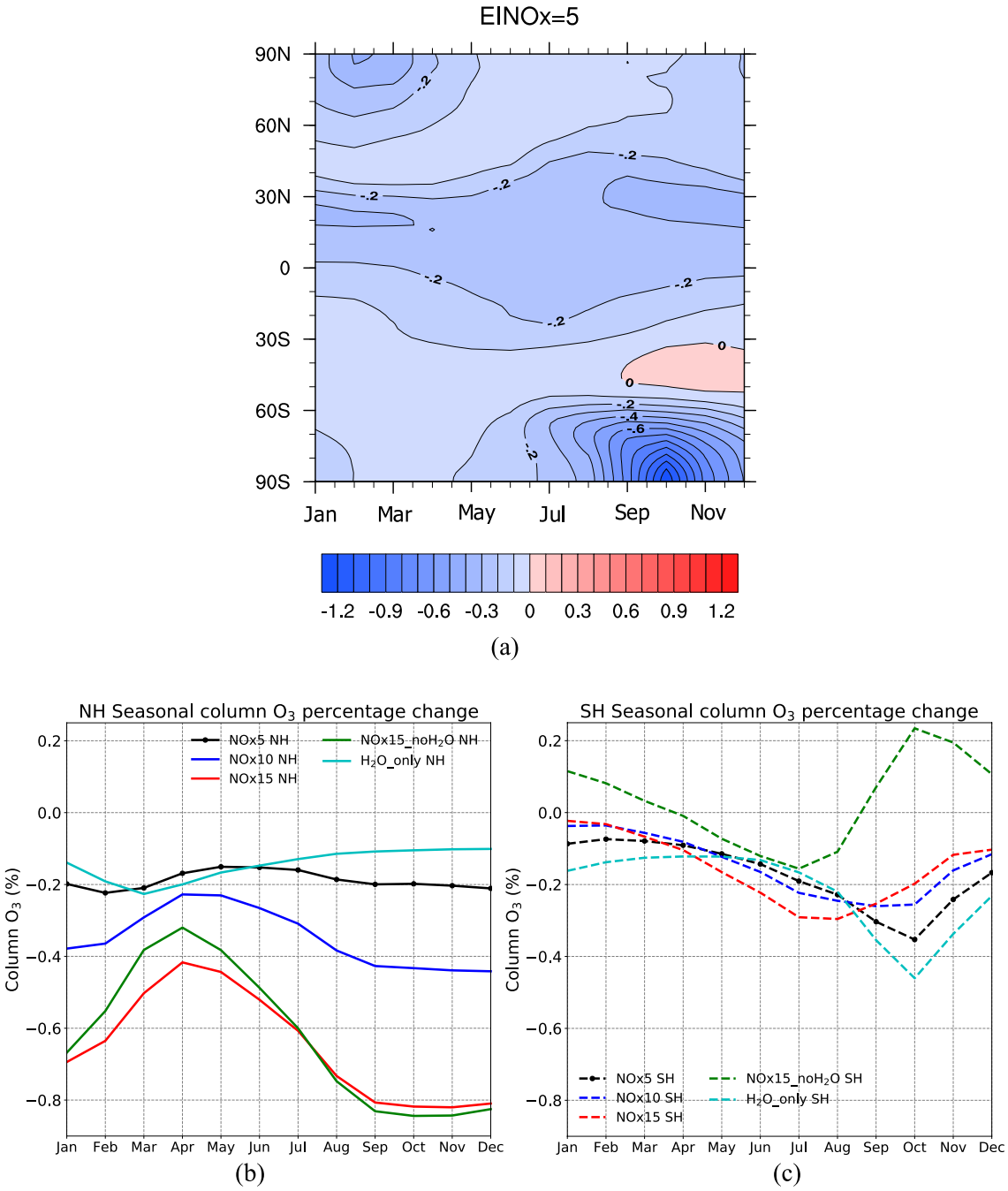

Figure 8. Calculated changes in seasonal dependence of total column ozone (%) for (a) baseline emission scenario (Case A); (b and c) for Case A and comparison to other emission scenarios in the Northern and Southern Hemisphere, respectively. The baseline emission scenario is shown in black lines with circles.

cycle. The definition of O_x and the reactions included in each catalytic cycle are based on the information in Brasseur and Solomon (2005) which also can be found in Text S1. The hemispheric averaging chemical loss rate is shown here for both the background conditions and for the change due to the perturbations (calculated from perturbed emission scenarios relative to background atmosphere). The results are shown for both hemispheres to explore the different behaviors of each catalytic cycle in both hemispheres (Figure S8). The Northern Hemispheric average chemical loss rate for the background conditions (Figure 6a) indicates that the NO_x involved O_x loss cycle (NO_x–O_x) and HO_x involved O_x loss cycle (HO_x–O_x) both play important

roles on the total O_x loss at different heights, with NO_x–O_x between 30 to 40 km and HO_x–O_x above 40 km, respectively. The loss from O_x self-loss cycle (O_x–O_x) and ClO_x/BrO_x involved O_x loss cycle (ClO_x/BrO_x–O_x) are important from 30 to 50 km, but to a much less degree compared to NO_x–O_x and HO_x–O_x cycles.

Figure 6 indicates that the reaction rates of all the O_x chemical loss cycles are modified even though only NO_x and H_2O emissions are injected into the atmosphere from HSCTs; this is expected since ozone is affected by the coupling of HO_x, NO_x and ClO_x/BrO_x chemistry. Although the emissions occur at 17–20 km, the effects on ozone are mostly above the emission levels. In the baseline Case A (Figure 6b), NO_x–O_x and HO_x–O_x cycles induced from NO_x and H_2O emissions together contribute to the majority of total O_x loss in both hemispheres. NO_x–O_x loss cycle dominates the O_x loss between 20 and 35 km, while HO_x–O_x starts to play a more significant role at higher altitudes from 40 to 50 km. The maximum of NO_x–O_x loss takes place at around 30 km, and the maximum of HO_x–O_x loss occurs at around 45 km. The hemispheric variance of total O_x loss primarily results from NO_x–O_x cycle with larger depletion in the NH where the emission occurs.

In Case B and C (Figure S8), similar to Case A, where NO_x and H_2O emit simultaneously, NO_x–O_x and HO_x–O_x cycles both contribute to the majority of total O_x loss in both hemispheres, while the effects from NO_x become more dominant as its emission level increases from 5 to 15 g/kg fuel. In addition, the ozone profile becomes more positive between 10 and 20 km, and more negative between 20 and 30 km with increasing $EINO_x$ from 5 to 15 g/kg (Figure 5b). For the pure NO_x or H_2O emission cases (Case D and E), the emitted species is the main source of odd-oxygen loss while the loss from other cycles tends to be reduced. The O_x loss by the HO_x–O_x and NO_x–O_x cycles both decrease when both NO_x and H_2O are emitted compared to the cases where they are emitted separately (Case C, D, and E); NO_x and HO_x can react to form longer-lived nitric acid, which reduces the overall O_x loss from HO_x–O_x and NO_x–O_x cycles.

Pure odd-oxygen loss (O_x–O_x) decreases in all cases due to the self-healing effects, that is, more O_x is destroyed by NO_x and/or HO_x cycles, leaving less O_x for the self-destruction process. The halogen involved O_x loss increases when there is HSCT H_2O emissions and the effect is stronger in the SH than NH. It is interesting to note that there is larger decrease in HO_x–O_x loss between 10 and 25 km in the NH compared to the SH when there is HSCT NO_x emissions (Figures 6c and 6d). Also, the NO_x–O_x loss cycle has a larger discrepancy between the NH and SH than the HO_x–O_x loss cycle, with greater NO_x–O_x loss in the NH where the primary emissions occur. The O_x loss from the HO_x–O_x cycle has little variance between the two hemispheres due to the majority of HO_x–O_x loss taking places at higher altitudes where more emission can transport across the equator to the SH.

Total column ozone change is calculated by integrating the changes in absolute ozone with altitude as shown in Figure 5. The net column ozone change determines the changes in the amount of biologically harmful ultraviolet radiation penetrating to the surface. The annually averaged change in total column ozone with latitude and longitude is shown in Figure 7; in this figure, the ozone reduction is partially offset by the ozone increase near the tropopause. Figure 7 does not show the strong zonal asymmetry seen in the map of emissions (Figure 1; this is largely related to the time scales for the transport processes that effectively spread out the ozone effects away from the source regions. There is a net decrease in total column ozone for the entire NH for all of the emissions scenarios due to catalytic cycles connected to NO_x and H_2O emissions. For Case A, B, C, and D, the ozone column depletion maxima occur at around 30°N where the majority of emissions occur. For the H_2O only, the peaks of ozone depletion are located at high southern latitudes. Slight increases (0.1%) in column ozone are found over the SH midlatitudes in Case B and C, and a greater increase (0.3%) in Case D is shown at mid to high latitudes. Notice that H_2O emissions are more responsible for ozone loss in the SH when considering the combined effects from the HSCT NO_x and H_2O emissions (Case C and D in Figure 7b).

Figure 8 shows the seasonal dependence of calculated percentage change in total column ozone with latitude. For Case A, total column ozone depletion occurs over most of the globe for the entire year, with the exception of a slight ozone increase at the SH midlatitudes in Spring (September to November). The peaks of ozone loss in both hemispheres occur in the springtime at the polar regions, with a maximum of −0.4% in NH March and −1.2% in SH October. The maximum total column ozone depletion at the South Pole is greater than at the North Pole for Case A due to stronger cancellation effects from ozone production and

Table 2
Percentage Changes (%) in Total Column Ozone for the WACCM Results Relative to the Earlier NASA AEAP and IPCC Aviation Assessment Results Taken From Kawa et al. (1999) and Penner et al. (1999)

Models	Case A $EINO_x = 5$ with H_2O	Case B $EINO_x = 10$ with H_2O	Case C $EINO_x = 15$ with H_2O	Case D $EINO_x = 15$ without H_2O	Case E $EINO_x = 0$ H_2O only	Case F $EINO_x = 5$ with H_2O Fleet 1,000
AER 2D	−0.3, −0.1	−0.3, −0.1	−0.3, −0.05	–	−0.6, −0.3	−0.7, −0.3
GSFC 2D	−0.4, −0.8	−0.6, −0.7	−0.8, −0.7	–	−0.4, −0.8	−0.9, −1.4,
LLNL 2D	−0.2, −0.2	−0.3, −0.1	−0.4, −0.01	–	−0.3, −0.3	−0.5, −0.3
CSIRO 2D	−0.2, −0.1	−0.3, −0.2	−0.5, −0.3	–	−0.2, −0.07	−0.5, −0.2
UNIVAQ 2D	−0.002, +0.02	+0.2, +0.1	+0.4, +0.2	–	−0.4, −0.2	−0.06, +0.005
SUNY 2D	−0.2, −0.1	−0.2, −0.06	–	–	−0.2, −0.1	−0.3, −0.2
THINAIR 2D	−0.2, −0.2	−0.5, −0.3	−0.9, −0.5	–	–	−0.4, −0.3
GMI 3D	+0.2, +0.05	–	–	–	–	–
LaRC 3D	−0.05, −0.1	+0.07, −0.03	–	–	–	–
SLIMCAT 3D	−0.4, −0.6	−0.5, −0.7	–	–	−0.6, −0.7	–
This study	**−0.21, -0.13**	**−0.38, -0.11**	**−0.66, -0.14**	**−0.62, −0.003**	**−0.13, −0.16**	**−0.45, -0.27**

Note. The first and second value is for the Northern Hemisphere (NH) and Southern Hemisphere (SH) average percent change in total column ozone, respectively.

reduction at the North Pole (as was shown in Figure 5a). The overall total column ozone depletion in the NH (−0.21%) is larger than that in the SH (−0.13%; Table 2). For Case A, the zonally averaged ozone change derived by WACCM are similar to several of the 2-D models from the NASA AEAP assessment (Figure S9), with the LLNL-2D model results coming closest to the WACCM results.

The reduction of total column ozone over the entire NH found in Figure 7 is confirmed in Figure 8b, and this is found for all seasons in all emission scenarios. In the NH, the maximum ozone depletion is found in the winter season for all cases except the H_2O emissions only case, where the maximum ozone depletion occurs in spring. In the SH, with the exception of Case D without H_2O emissions, all of the other cases have maximum ozone depletion occurring in the late winter and spring seasons from August to November. Cases with H_2O emission also have larger ozone depletion in the SH than the case without H_2O emission (Case D). The H_2O emissions can increase the surface area density of ice over the stratosphere in the SH high latitudes region, contributing to this behavior (see Figure S10). The surface area density increase further promotes the heterogeneous ozone depletion catalytic cycles occurring on the surface of ice particles in spring (Molina et al., 1987; Solomon, 1999). This is shown by Figure S11, where the reaction rates of halogen involved heterogeneous reactions on ice particles show a large increase with the same pattern as the increase of surface area density of ice particle (Figure S11) during the time period when ozone depletion peaks in the SH. This is the same ozone depletion mechanism that causes the Antarctic ozone hole (WMO, 2018).

4.3. Indirect Effects of HSCT Fleet on Climate Forcing from Ozone and Water Vapor

The impact of an HSCT fleet on climate is associated with its emissions of CO_2, H_2O, NO_x, SO_2, and soot. For CO_2 emission, using 5.137×10^{18} kg as the mass of the atmosphere (Trenberth, 1981), the fuel consumption of 500 HSCT aircraft can induce the increase of atmospheric CO_2 0.019 ppmv, with a radiative forcing of 4.1 mW/m^2, respectively (Myhre et al., 1998). This CO_2 emission from the fleet would be too small to have a meaningful impact on stratospheric temperatures. Previous 1999 NASA and IPCC assessments have also indicated that the contribution of HSCTs to global radiative forcing change would likely have larger impact from the perturbations in stratospheric H_2O and ozone than from CO_2 emission. The NO_x and H_2O emissions can also lead to an increase in tropospheric ozone and tropospheric OH concentration, which further decreases the lifetime of methane. Previous study indicates that the reduction of methane lifetime is a minor secondary effect (Grewe, Stenke, et al., 2007). In this study, we only focus on evaluating the potential radiative forcing impact of the H_2O and O_3 perturbation from H_2O and NO_x emissions. The stratospheric

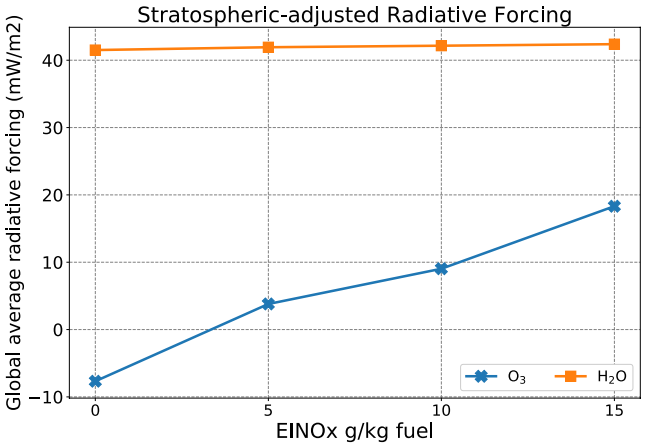

Figure 9. Annual average change in stratospheric-adjusted radiative forcing (mW/m^2) as a function of NO_x emission levels for fleets of HSCTs based on the changes in H_2O and O_3.

H_2O released from HSCT emissions is a strong greenhouse gas associated with a warming effect on the surface. On the other hand, NO_x and H_2O emissions can both perturb stratospheric ozone. The chemically induced ozone depletion in the stratosphere will cool both the surface and the stratosphere, and vice versa the chemically induced ozone production will warm both the surface and stratosphere.

The radiative forcing calculated in this study is the stratospheric-adjusted radiative forcing, which is more relevant to surface temperature change than just deriving the instantaneous forcing. To calculate the stratospheric-adjusted radiative forcing, the stratosphere is allowed to relax to the thermal steady state, leaving an energy imbalance only in the troposphere system. Once the stratosphere has been allowed to adjust to a forcing, the change in energy flux at the tropopause is equivalent to that at the top of the atmosphere.

The forcings of H_2O and ozone perturbations are treated separately in different cases as adding them up can offset the warming and cooling effects induced individually. Figure 9 indicates the stratospheric-adjusted radiative forcing (mW/m^2) as a function of NO_x emission levels. For stratospheric H_2O perturbation, all of the cases with H_2O emissions indicate a warming impact on the surface. The derived forcing is consistent for Case A, B, C, and E with a forcing of ~42 mW/m^2, as these cases have the same H_2O emissions (Table S3). The H_2O forcing is negligible for Case D as there is no H_2O emission. A forcing of 74 mW/m^2 is calculated for Case F with the increasing H_2O perturbation from doubling the number of HSCT aircraft in operation, which falls into the range of 30–300 mW/m^2 derived by different models from the earlier 1999 NASA and IPCC assessments.

Forcing changes for perturbed ozone are more complicated than H_2O. For the ozone perturbations, all cases indicate a warming impact on the surface except for Case E (H_2O only). As shown in Figure 9, the magnitude of warming increases as the HSCT NO_x emissions increase from 5 to 15 g/kg fuel, with a net positive forcing ranging from 2 to 20 mW/m^2. The net forcing effects from ozone perturbation results from two competing processes. The ozone depletion in the stratosphere results in a cooling effect. At the same time, the ozone increase in the troposphere due to NO_x emission induces a warming effect at the surface. For Case A, B, C, D, and F, the warming caused by the tropospheric ozone increase dominates over the cooling induced by stratospheric ozone depletion despite the net reduction in total column ozone, resulting in a net warming effect. While for H_2O only emission (Case E), there is no ozone increase in the troposphere and therefore the stratospheric ozone depletion alone leads to a net negative forcing of ~−8 mW/m^2. For a fleet of 1,000 with $EINO_x = 5$ (Case F), this study calculated a radiative forcing of 2 mW/m^2, which is in the range from −50 to 10 mW/m^2 provided by different models from the earlier 1999 NASA and IPCC assessments.

5. Comparison to the Earlier Supersonic Aircraft Assessments

The calculated total column ozone percentage change from the HSCT emission scenarios are shown in Table 2 for different NO_x emission indexes and fleet sizes in a 2015 background atmosphere. The results from the earlier 1999 NASA AEAP and IPCC aviation assessments (Kawa et al, 1999; Penner et al., 1999) using 2-D and 3-D models from that time period are shown here for comparison. The calculated percentage change in total column ozone from this study with WACCM is shown in the last row. All total column ozone changes are shown here for each emission scenario relative to the subsonic only background atmosphere. The maximum global average ozone depletion calculated in this study is around −0.4% (Case C), which is 8% of the maximum historical ozone percentage depletion (around −5%) occurring after the Pinatubo volcano eruption in 1992.

The results are more similar to the earlier results from the 2-D models than the early stage 3-D models. For the baseline scenario Case A, this study determines a change in percentage ozone of −0.21% and −0.13% for the NH and SH, respectively. This change falls into the range of +0.2 to −0.4% in the NH and +0.05 to −0.8 in the SH calculated from previous models shown in Table 2. For Cases B and C, with increasing $EINO_x$ to

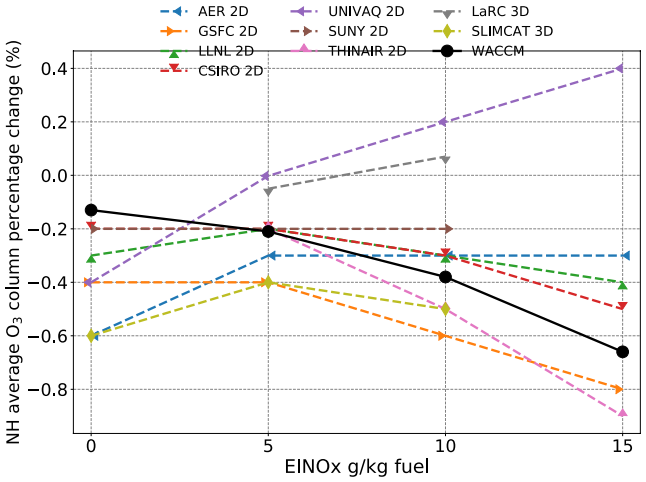

Figure 10. Northern Hemisphere total ozone column change (%) as a function of $EINO_x$ for a fleet size of 500 supersonic aircraft. Results from earlier models are shown in dashed lines while the WACCM results are shown in solid black line.

either 10 or 15 g NO_2/kg fuel, the WACCM derived ozone loss in the NH tends to be larger than that from most of the earlier models. Case D, for only NO_x emissions with $EINO_x = 15$, was not considered in the earlier assessments.

For the H_2O only emissions scenario Case E, the WACCM results are lower than all of the earlier models in the NH. Doubling the fleet to 1,000 HSCTs assumed to be in operation (Case F), the total column ozone percentage change calculated from WACCM is −0.45% and −0.27% in the NH and SH respectively, which is in the range of values calculated from previous models.

Figure 10 shows the sensitivity of ozone depletion in the NH as a function of NO_x emission indices for a fleet of 500 supersonic aircraft calculated from WACCM and the comparison to earlier models. Results for the SH is shown in Figure S12. In general, WACCM derives a higher sensitivity in the NH between the levels of NO_x emissions and the resulting ozone changes. As the NO_x emission index goes from no NO_x emission (the H_2O only perturbation case) to 5 g/kg fuel) WACCM has a higher sensitivity in ozone depletion than all of the earlier models. Increasing the NO_x emission index from 5 to 15 g/kg fuel also shows WACCM having a stronger sensitivity compared to most of the earlier models, with one exception, the THINAIR 2D model.

6. Conclusions

To better explore the environmental effects from potential future fleets of SST aircraft, we revisited prior studies that evaluated the HSCTs effects, especially those from the last major assessment of potential impacts done about 20 years ago. This study establishes a baseline relative to the earlier NASA and IPCC assessments, and determines the potential environmental effects from NO_x and H_2O emissions for a fleet of SST aircraft. Using the state-of-the-art whole chemistry climate model WACCM with the most recent NASA JPL chemistry recommendations and a much-improved representation of atmospheric dynamics and transport, this study provides an update relative to those earlier results from NASA and IPCC assessments.

In general, the results derived from WACCM are more similar to results from the 2-D models used in the earlier assessments than to the results from the early stage 3-D models used in those assessments. For the baseline emission scenario (a fleet of 500 with $EINO_x = 5$ g/kg fuel at a Mach number 2.4), WACCM determines a global annual average decrease in total column ozone of −0.17%, similar to findings from several of the earlier 2-D models (Table 2). Further exploring the ozone sensitivity to NO_x emission levels, WACCM derives a greater sensitivity to NO_x than found in the earlier models. The difference in results can be attributed to the significant improvements in representation of atmospheric chemistry and physical processes in WACCM, including incorporating a better description of stratosphere-troposphere exchange than the earlier models. Proper treatment of these processes is particularly important for considering supersonic cruise impacts at lower Mach numbers where the emissions would be closer to the tropopause.

Detailed analysis of the ozone perturbations found that the NO_x and H_2O emissions from a fleet of HSCTs can potentially have a strong impact on stratospheric ozone and climate. An ozone increase region for these perturbations is found near the tropopause; this increase is due to the combined effects from a reduction in ozone loss rates due to interference reactions and the direct effects of enhanced ozone production from NO_x emissions. Ozone depletion maximizes at cruise altitudes in the NH where the majority of the emissions occur. The ozone depletion in the stratosphere is partly mitigated by an ozone increase in lower altitudes resulting in a less dramatic net column ozone impact. Depending on the amounts of NO_x and H_2O emissions and the resulting chemical interactions between all the ozone destroying catalytic cycles, the maximum global annual average column ozone depletion reaches −0.4% from a range of emission scenarios evaluated in this study. This depletion is 8% of the maximum historical ozone depletion of −5% occurring after the Pinatubo volcano eruption in 1992. From analysis of the radiative forcing impact, we confirm that

stratospheric H_2O emissions are an important factor in potential climate impacts from supersonic aircraft emissions.

Data Availability Statement

The atmospheric modeling data sets used in the development of the tables and figures from this study are available to the community through the Illinois Data Bank (IDB), a public access repository at the University of Illinois at Urbana-Champaign (UIUC). The website for our data set at the University of Illinois Data Bank is: https://databank.illinois.edu/datasets/IDB-9081595.

Acknowledgments
The authors thank Simone Tilmes for helping with SST/ICE data files to drive the WACCM simulations, and Jean-Francois Lamarque and Francis Vitt for providing suggestions on running PORT. The authors acknowledge the high-performance computing support provided by NCAR's Computational and Information Systems Laboratory, sponsored by the National Science Foundation. The University of Illinois received support in part from the Boeing Company and from the U.S. Federal Aviation Administration (13-C-AJFE-UI-029).

References

Baughcum, S. L., & Henderson, S. C. (1995). *Aircraft emission inventories projected in year 2015 for a high speed civil transport (HSCT) universal airline network*. NASA CR-4659.

Baughcum, S. L., & Henderson, S. C. (1998). *Aircraft emission scenarios projected in year 2015 for the NASA Technology Concept Aircraft (TCA) high speed civil transport*. NASA CR-1998-207635.

Baughcum, S. L., Henderson, S. C., Hertel, P. S., Maggiora, D. R., & Oncina, C. A. (1994). *Stratospheric emissions effects database development*. NASA CR-4592. Retrieved from https://ntrs.nasa.gov/

Brasseur, G. P., & Solomon, S. (2005). *Aeronomy of the middle atmosphere*. Atmospheric and Oceanographic Science Library (Vol. 32). Dordrecht, The Netherlands: Springer.

Conley, A. J., Lamarque, J. F., Vitt, F., Collins, W. D., & Kiehl, J. (2013). PORT, a CESM tool for the diagnosis of radiative forcing. *Geoscientific Model Development*, *6*(2), 469–476. https://doi.org/10.5194/gmd-6-469-2013

Crutzen, P. J. (1972). SST's: A threat to the earth's ozone shield. *Ambio*, 41–51.

Dameris, M., Grewe, V., Köhler, I., Sausen, R., Brühl, C., Grooß, J. U., & Steil, B. (1998). Impact of aircraft NO_x emissions on tropospheric and stratospheric ozone. Part II: 3-D model results. *Atmospheric Environment*, *32*(18), 3185–3199. https://doi.org/10.1016/S1352-2310(97)00505-0

DeMore, W. B., Sander, S. P., Golden, D. M., Hampson, R. F., Kurylo, M. J., Howard, C. J., et al. (1997). *Chemical kinetics and photochemical data for use in stratospheric modeling*. JPL Publication 97-4. Pasadena, CA: Jet Propulsion Laboratory.

Dessens, O., Rogers, H. L., & Pyle, J. A. (2007). A change in the calculated impact of supersonic aircraft NO_x emissions on the atmosphere. *The Aeronautical Journal*, *111*(1119), 311–314. https://doi.org/10.1017/S0001924000004553

Fahey, D. W., Keim, E. R., Boering, K. A., Brock, C. A., Wilson, J. C., Jonsson, H. H., et al. (1995). Emission measurements of the Concorde supersonic aircraft in the lower stratosphere. *Science*, *270*(5233), 70–74. https://doi.org/10.1126/science.270.5233.70

Fels, S. B., Mahlman, J. D., Schwarzkopf, M. D., & Sinclair, R. W. (1980). Stratospheric sensitivity to perturbations in ozone and carbon dioxide: Radiative and dynamical response. *Journal of the Atmospheric Sciences*, *37*(10), 2265–2297.

Froidevaux, L., Anderson, J., Wang, H. J., Fuller, R. A., Schwartz, M. J., Santee, M. L., et al. (2015). Global OZone Chemistry And Related trace gas Data records for the Stratosphere (GOZCARDS): Methodology and sample results with a focus on HCl, H_2O, and O_3. *Atmospheric Chemistry and Physics*, *15*(18), 10471–10507. https://doi.org/10.5194/acp-15-10471-2015

Froidevaux, L., Kinnison, D. E., Wang, R., Anderson, J., & Fuller, R. A. (2019). Evaluation of CESM1 (WACCM) free-running and specified dynamics atmospheric composition simulations using global multispecies satellite data records. *Atmospheric Chemistry and Physics*, *19*(7), 4783–4821. https://doi.org/10.5194/acp-19-4783-2019

Garcia, R. R., Smith, A. K., Kinnison, D. E., Cámara, Á. D. L., & Murphy, D. J. (2017). Modification of the gravity wave parameterization in the Whole Atmosphere Community Climate Model: Motivation and results. *Journal of the Atmospheric Sciences*, *74*(1), 275–291. https://doi.org/10.1175/JAS-D-16-0104.1

Garcia, R. R., Yue, J., & Russell, J. M., III (2019). Middle atmosphere temperature trends in the twentieth and twenty-first centuries simulated with the Whole Atmosphere Community Climate Model (WACCM). *Journal of Geophysical Research: Space Physics*, *124*(10), 7984–7993. https://doi.org/10.1029/2019JA026909

Gettelman, A., Holton, J. R., & Rosenlof, K. H. (1997). Mass fluxes of O_3, CH_4, N_2O and CF_2Cl_2 in the lower stratosphere calculated from observational data. *Journal of Geophysical Research*, *102*(D15), 19149–19159. https://doi.org/10.1029/97JD01014

Grewe, V., Plohr, M., Cerino, G., Di Muzio, M., Deremaux, Y., Galerneau, M., et al. (2010). Estimates of the climate impact of future small-scale supersonic transport aircraft – Results from the HISAC EU-project. *The Aeronautical Journal*, *114*(1153), 199–206. Retrieved from https://elib.dlr.de/64106/

Grewe, V., Stenke, A., Ponater, M., Sausen, R., Pitari, G., Iachetti, D., et al. (2007). Climate impact of supersonic air traffic: An approach to optimize a potential future supersonic fleet – Results from the EU-project SCENIC. *Atmospheric Chemistry and Physics*, *7*(19), 5129–5145. https://doi.org/10.5194/acp-7-5129-2007

Grooß, J. U., Brühl, C., & Peter, T. (1998). Impact of aircraft emissions on tropospheric and stratospheric ozone. Part I: Chemistry and 2-D model results. *Atmospheric Environment*, *32*(18), 3173–3184. https://doi.org/10.1016/S1352-2310(98)00016-8

Holton, J. R., Haynes, P. H., McIntyre, M. E., Douglass, A. R., Rood, R. B., & Pfister, L. (1995). Stratosphere-troposphere exchange. *Reviews of Geophysics*, *33*(4), 403–439. https://doi.org/10.1029/95RG02097

IPCC. (2013). *The physical science basis. Contribution of working group I to the fifth assessment report of IPCC the intergovernmental panel on climate change* (p. 1535). Cambridge, UK: Cambridge University Press.

Ivy, D. J., Hilgenbrink, C., Kinnison, D., Alan Plumb, R., Sheshadri, A., Solomon, S., & Thompson, D. W. (2017). Observed changes in the Southern Hemispheric circulation in May. *Journal of Climate*, *30*(2), 527–536. https://doi.org/10.1175/JCLI-D-16-0394.1

Johnston, H. (1971). Reduction of stratospheric ozone by nitrogen oxide catalysts from supersonic transport exhaust. *Science*, *173*(3996), 517–522. https://doi.org/10.1126/science.173.3996.517

Johnston, H. S., Kinnison, D. E., & Wuebbles, D. J. (1989). Nitrogen oxides from high-altitude aircraft: An update of potential effects on ozone. *Journal of Geophysical Research: Atmospheres*, *94*(D13), 16351–16363. https://doi.org/10.1029/JD094iD13p16351

Kawa, S. R., Anderson, J. G., Baughcum, S. L., Brock, C. A., Brune, W. H., Cohen, R. C., et al. (1999). *Assessment of the effects of high-speed aircraft in the stratosphere: 1998* (National Aeronautics and Space Administration report). NASA/TMM1999-209237.

Kinnison, D., Brasseur, G., Baughcum, S. L., Zhang, J., & Wuebbles, D. (2020). The impact on the ozone layer of a potential fleet of civil hypersonic aircraft. *Earth's Future*, *8*(10), e2020EF001626. https://doi.org/10.1029/2020EF001626

Kinnison, D. E., Brasseur, G. P., Walters, S., Garcia, R. R., Marsh, D. R., Sassi, F., et al. (2007). Sensitivity of chemical tracers to meteorological parameters in the MOZART-3 chemical transport model. *Journal of Geophysical Research: Atmospheres*, *112*(D20). https://doi.org/10.1029/2006JD007879

Kinnison, D. E., Connell, P. S., Rodriguez, J. M., Rotman, D. A., Considine, D. B., Tannahill, J., et al. (2001). The Global Modeling Initiative assessment model: Application to high-speed civil transport perturbation. *Journal of Geophysical Research*, *106*(D2), 1693–1711. https://doi.org/10.1029/2000JD900406

Kinnison, D. E., & Wuebbles, D. J. (1994). *Impact of supersonic and subsonic aircraft on ozone: Including heterogeneous chemical reaction mechanisms* (National Aeronautics and Space Administration report). NASA N95-10666.

Kloss, C., Newland, M. J., Oram, D. E., Fraser, P. J., Brenninkmeijer, C. A., Röckmann, T., & Laube, J. C. (2014). Atmospheric abundances, trends and emissions of CFC-216ba, CFC-216ca and HCFC-225ca. *Atmosphere*, *5*(2), 420–434. https://doi.org/10.3390/atmos5020420

Kunz, A., Pan, L. L., Konopka, P., Kinnison, D. E., & Tilmes, S. (2011). Chemical and dynamical discontinuity at the extratropical tropopause based on START08 and WACCM analyses. *Journal of Geophysical Research*, *116*(D24). https://doi.org/10.1029/2011JD016686

Lamarque, J. F., Kyle, G. P., Meinshausen, M., Riahi, K., Smith, S. J., van Vuuren, D. P., et al. (2011). Global and regional evolution of short-lived radiatively-active gases and aerosols in the Representative Concentration Pathways. *Climatic Change*, *109*(1–2), 191–212. https://doi.org/10.1007/s10584-011-0155-0

Livesey, N. J., Read, W. G., Wagner, P. A., Froidevaux, L., Lambert, A., Manney, G. L., et al. (2015). *EOS MLS Version 4.2 x Level 2 data quality and description document*. Pasadena, CA: Jet Propulsion Laboratory, California Institute of Technology.

Marsh, D. R., Mills, M. J., Kinnison, D. E., Lamarque, J. F., Calvo, N., & Polvani, L. M. (2013). Climate change from 1850 to 2005 simulated in CESM1 (WACCM). *Journal of Climate*, *26*(19), 7372–7391. https://doi.org/10.1175/JCLI-D-12-00558.1

Matthes, K., Marsh, D. R., Garcia, R. R., Kinnison, D. E., Sassi, F., & Walters, S. (2010). Role of the QBO in modulating the influence of the 11 year solar cycle on the atmosphere using constant forcings. *Journal of Geophysical Research*, *115*(D18). https://doi.org/10.1029/2009JD013020

Meinshausen, M., Smith, S. J., Calvin, K., Daniel, J. S., Kainuma, M. L. T., Lamarque, J. F., et al. (2011). The RCP greenhouse gas concentrations and their extensions from 1765 to 2300. *Climatic Change*, *109*(1–2), 213. https://doi.org/10.1007/s10584-011-0156-z

Molina, M. J., Tso, T. L., Molina, L. T., & Wang, F. C. Y. (1987). Antarctic stratospheric chemistry of chlorine nitrate, hydrogen chloride, and ice: Release of active chlorine. *Science*, *238*(4831), 1253–1257. https://doi.org/10.1126/science.238.4831.1253

Morgenstern, O., Hegglin, M. I., Rozanov, E., O'Connor, F. M., Abraham, N. L., Akiyoshi, H., et al. (2017). Review of the global models used within phase 1 of the Chemistry-Climate Model Initiative (CCMI). *Geoscientific Model Development*, *10*(2), 639–671. https://doi.org/10.5194/gmd-10-639-2017

Myhre, G., Highwood, E. J., Shine, K. P., & Stordal, F. (1998). New estimates of radiative forcing due to well mixed greenhouse gases. *Geophysical Research Letters*, *25*(14), 2715–2718. https://doi.org/10.1029/98GL01908

Park, M., Randel, W. J., Kinnison, D. E., Bourassa, A. E., Degenstein, D. A., Roth, C. Z., et al. (2017). Variability of stratospheric reactive nitrogen and ozone related to the QBO. *Journal of Geophysical Research: Atmospheres*, *122*(18), 10103–10118. https://doi.org/10.1002/2017JD027061

Penner, J. E., Lister, D. H., Griggs, D. J., Dokken, D. J., & McFarland, M. (Eds.). (1999). *Aviation and the global atmosphere* (pp. 1–373). Cambridge, UK: Cambridge University Press.

Polvani, L. M., Previdi, M., England, M. R., Chiodo, G., & Smith, K. L. (2020). Substantial twentieth-century Arctic warming caused by ozone-depleting substances. *Nature Climate Change*, *10*(2), 130–133. https://doi.org/10.1038/s41558-019-0677-4

Prinn, R. G., Weiss, R. F., Arduini, J., Arnold, T., DeWitt, H. L., Fraser, P. J., et al. (2018). History of chemically and radiatively important atmospheric gases from the Advanced Global Atmospheric Gases Experiment (AGAGE). *Earth System Science Data Discussions*, *10*(2), 985–1018. https://doi.org/10.5194/essd-10-985-2018

Remsberg, E. E., Marshall, B. T., Garcia-Comas, M., Krueger, D., Lingenfelser, G. S., Martin-Torres, J., et al. (2008). Assessment of the quality of the Version 1.07 temperature-versus-pressure profiles of the middle atmosphere from TIMED/SABER. *Journal of Geophysical Research*, *113*(D17). https://doi.org/10.1029/2008JD010013

Sander, S. P., Abbatt, J., Barker, J. R., Burkholder, J. B., Friedl, R. R., Golden, D. M., et al. (2010). *Chemical Kinetics and Photochemical Data for Use in Atmospheric Studies, Evaluation No. 17*. JPL Publication 10-6.

Shepherd, T. G., & McLandress, C. (2011). A robust mechanism for strengthening of the Brewer–Dobson circulation in response to climate change: Critical-layer control of subtropical wave breaking. *Journal of the Atmospheric Sciences*, *68*(4), 784–797. https://doi.org/10.1175/2010JAS3608.1

Solomon, S. (1999). Stratospheric ozone depletion: A review of concepts and history. *Reviews of Geophysics*, *37*(3), 275–316. https://doi.org/10.1029/1999RG900008

Solomon, S., Ivy, D. J., Kinnison, D., Mills, M. J., Neely, R. R., & Schmidt, A. (2016). Emergence of healing in the Antarctic ozone layer. *Science*, *353*(6296), 269–274. https://doi.org/10.1126/science.aae0061

Solomon, S., Kinnison, D., Bandoro, J., & Garcia, R. (2015). Simulation of polar ozone depletion: An update. *Journal of Geophysical Research: Atmospheres*, *120*(15), 7958–7974. https://doi.org/10.1002/2015JD023365

Strahan, S. E. (1999). Climatologies of lower stratospheric NO_y and O_3 and correlations with N_2O based on in situ observations. *Journal of Geophysical Research*, *104*(D23), 30463–30480. https://doi.org/10.1029/1999JD900775

Swinbank, R., & Ortland, D. A. (2003). Compilation of wind data for the Upper Atmosphere Research Satellite (UARS) reference atmosphere project. *Journal of Geophysical Research*, *108*(D19). https://doi.org/10.1029/2002JD003135

Trenberth, K. E. (1981). Seasonal variations in global sea level pressure and the total mass of the atmosphere. *Journal of Geophysical Research*, *86*(C6), 5238–5246. https://doi.org/10.1029/JC086iC06p05238

Wang, R., Froidevaux, L., Anderson, J., Fuller, R. A., Bernath, P. F., McCormick, M. P., et al. (2013). *GOZCARDS Merged Ozone 1 month L3 10 degree Zonal Means on a Vertical Pressure Grid V1*. Greenbelt, MD, USA: Goddard Earth Sciences Data and Information Services Center.

Wang, Y., & Huang, Y. (2020). Understanding the atmospheric temperature adjustment to CO_2 perturbation at the process level. *Journal of Climate*, *33*(3), 787–803. https://doi.org/10.1175/JCLI-D-19-0032.1

Wegner, T., Kinnison, D. E., Garcia, R. R., & Solomon, S. (2013). Simulation of polar stratospheric clouds in the specified dynamics version of the whole atmosphere community climate model. *Journal of Geophysical Research: Atmospheres*, *118*(10), 4991–5002. https://doi.org/10.1002/jgrd.50415

Werner, B., Stutz, J., Spolaor, M., Scalone, L., Raecke, R., Festa, J., et al. (2017). Probing the subtropical lowermost stratosphere and the tropical upper troposphere and tropopause layer for inorganic bromine. *Atmospheric Chemistry and Physics*, *17*(2), 1161–1186. https://doi.org/10.5194/acp-17-1161-2017

World Meteorological Organization (WMO) (2018). *Scientific assessment of ozone depletion: 2018* (Global Ozone Research and Monitoring Project-Report No. 58, p. 588). Geneva, Switzerland: World Meteorological Organization.

Technical Report Documentation Page

1. Report No.	2. Government Accession No.	3. Recipient's Catalog No.
2020JD034130		

4. Title and Subtitle	5. Report Date
Potential Impacts of Supersonic Aircraft Emissions on Ozone and Resulting Forcing on Climate: An Update on Historical Analysis	February 2021
	6. Performing Organization Code

7. Author(s)	8. Performing Organization Report No.
Jun Zhang, Donald Wuebbles, Douglas Kinnison, Steven L. Baughcum	

9. Performing Organization Name and Address	10. Work Unit No. (TRAIS)
Center of Excellence for: Alternative Jet Fuels and Environment University of Illinois 105 S. Gregory Street, Urbana, IL 61801	11. Contract or Grant No. 13-C-AJFE-UI-029

12. Sponsoring Agency Name and Address	13. Type of Report and Period Covered
Federal Aviation Administration Office of Environment and Energy	Journal Article
	14. Sponsoring Agency Code

15. Supplementary Notes

16. Abstract

Commercial aircraft flying at supersonic speeds in the lower stratosphere are being discussed once again after a hiatus of almost 20 years. Potential environmental effects from fleets of such aircraft need to be understood for their possible impacts on stratospheric ozone; levels of stratospheric ozone determine the amount of biologically harmful ultraviolet radiation from the Sun reaching the Earth's surface. Changes in the distribution and concentrations of ozone also have implications on climate. This study evaluates the potential impact on stratospheric ozone and on climate forcing from different levels of nitrogen oxides (NOx) and water vapor (H2O) emissions from supersonic transport. Toward establishing a baseline relative to prior studies, we also compare these new analyses with results from the 1999 aviation assessments, using the same aviation emissions. Despite the understanding of atmospheric processes used in studying chemistry-climate interactions have been greatly enhanced over the last 20 years, this study finds that, for the baseline scenario, the resulting effects on stratospheric ozone are similar to those from many of the models in the prior assessment, although with a stronger ozone sensitivity to NOx emissions. We show that the resulting ozone effects largely depend on the NOx and H2O emission levels and the net changes in stratospheric ozone are determined by the chemical interactions between different ozone production and depletion cycles. We also calculate the radiative forcing impact for the resulting changes in the distributions of ozone and H2O, and confirm that stratospheric H2O emissions are an important factor in potential climate impacts from supersonic aircraft emissions.

17. Key Words	18. Distribution Statement
climate, ozone, supersonic aircraft, ASCENT	

19. Security Classif. (of this report)	20. Security Classif. (of this page)	21. No. of Pages	22. Price
Unclassified	Unclassified		